Structure, morphology, and optical properties of highly ordered films of *para*-sexiphenyl

E. Zojer* and N. Koch
Institut für Festkörperphysik, Technische Universität Graz, Petersgasse 16, A-8010 Graz, Austria

P. Puschnig
Institut für Theoretische Physik, Universität Graz, A-8010 Graz, Austria

F. Meghdadi, A. Niko, and R. Resel
Institut für Festkörperphysik, Technische Universität Graz, Petersgasse 16, A-8010 Graz, Austria

C. Ambrosch-Draxl
Institut für Theoretische Physik, Universität Graz, A-8010 Graz, Austria

M. Knupfer and J. Fink
Institut für Festkörper- und Werkstofforschung, Postfach 270016, D-01171 Dresden, Germany

J. L. Brédas
Service de Chimie des Matériaux Nouveaux, Centre de Recherche en Electronique et Photonique Moléculaires, Université de Mons-Hainaut, Place du Parc 20, B-7000 Mons, Belgium and Department of Chemistry, The University of Arizona, PO Box 210041, Tucson, Arizona 85721-0041

G. Leising
Institut für Festkörperphysic, Technische Universität Graz, Petersgasse 16, A-8010 Graz, Austria
(Received 22 June 1999; revised manuscript received 4 January 2000)

We have investigated the properties of highly textured films of para-sexiphenyl ($6P$). The films are obtained by evaporation in high vacuum with different deposition rates and substrate temperatures. The crystal structure is analyzed by x-ray and elastic electron diffraction. Depending on the evaporation conditions and on the substrate pretreatment we find a marked texturing of the films. To better understand the growth conditions of $6P$ we have analyzed the film morphology by atomic force microscopy. The optical properties in the ultraviolet and infrared range are studied as a function of the orientation of the molecules. This enables us to show a strong anisotropy of absorption, luminescence, and luminescence excitation spectra. In order to gain a better understanding of the optical-absorption spectrum of the $6P$ molecular crystals we have analyzed the properties of films with chains oriented parallel and perpendicular to the substrate surface at low temperatures using a He cryostat. Both orientation and temperature-dependent absorption experiments clearly show the very complex nature of the low-energy absorption spectrum of $6P$. To distinguish between intrinsic molecular properties and the effects of the three-dimensional crystal structure we have compared the experimental results to highly correlated post Hartree-Fock and to density functional theory (DFT) calculations for isolated $6P$ molecules as well as to angular dependent absorption spectra derived from DFT band structures.

I. INTRODUCTION

There is a steadily growing technological interest in conjugated organic materials due to the wide range of possible applications like light-emitting diodes (LED's),[1] light-emitting electrochemical cells (LEC's),[2] photodiodes, solar cells,[3] and also fully organic transistors.[4] Phenylene based materials are especially interesting because of their high quantum efficiencies[5,6] combined with emission in the blue spectral range interesting for LED[7,8] and laser applications.[9] They also allow the realization of red-green-blue full color displays via color conversion techniques.[10] Para-sexiphenyl ($6P$) plays a special role amongst those materials because it can be synthesized and purified in a well-defined way, the number of phenylene units along which the π electrons are delocalized is large enough to yield emission in the blue spectral range and homogenous films can be obtained by vacuum deposition.

In order to improve the performance of any kind of devices and to achieve novel applications like diodes emitting polarized light[8] (interesting e.g., for backlight applications) a detailed knowledge of the film growth as a function of substrate materials and evaporation conditions is essential. In this context it is not the primary goal of the present paper to focus on a systematic investigation of the $6P$ growth conditions on various substrates as a function of deposition rate and temperature (this has been studied e.g., in Ref. 11). It has rather been our intention to employ our knowledge about film growth in order to maximize the alignment of the $6P$ chains relative to a preferred direction to obtain highly textured films suitable for various kinds of orientation and polarization dependent spectroscopic investigations, which al-

TABLE I. Deposition conditions and resulting orientations for the investigated 6*P* samples.

Sample	Substrate material	Average evaporation rate (Å/min)	Substrate temperature	Average film thickness (nm)[a]	Determined texturing of chains
A	NaCl	1–2	Ambient temperature	120	Parallel to preferred direction induced by a preoriented layer on substrate
B	NaCl	1–2	150 °C	<190	72° tilted relative to film surface
C	quartz	1–2	100 °C	123	72° tilted+perpendicular to film surface
D	quartz	~200	Ambient temperature	88	Predominantly parallel to film surface

[a]For the films on the quartz substrates (*C,D*) the film thickness has been determined with a Tolansky interferometer, whereas the values for films *A* and *B* correspond to the readings from the microbalance in our evaporation setup. As the microbalance is not heated, the value obtained for film *B* can only be regarded as an upper limit to the actual film thickness.

low a deeper insight into the physical properties of the molecular crystals. We have grown films on NaCl substrates, for which a quasiepitaxial growth can be observed and which are also suitable to obtain samples with 6*P* chains lying parallel to the substrate surface in a direction induced by a rubbing process.[8] Films of high optical quality are grown on quartz substrates. The significant degree of anisotropy in the films is confirmed by x-ray and elastic electron diffraction and by Fourier-transform infrared (FTIR) spectroscopy. An investigation of the surface morphology of 6*P* layers[11] shows that, in contrast to the observations made for films deposited onto substrates held at room temperature, a layered growth prevails on a NaCl crystal held at 150 °C not only at the first monolayers but also for relatively thick films.

A dependence of the optical absorption spectrum of 6*P* on the evaporation conditions has been reported in a number of publications[12–14] and an evaluation of the directional dependence of the absorption spectrum has clearly shown that this effect has to be attributed to different orientations of the molecular axes relative to the direction of the incident light.[14] Similar experimental observations as for 6*P* have been made for the model oligomers of poly(thiophene).[15,16] In this paper we more deeply investigate the optical properties of 6*P* films by polarization and orientation dependent experiments on highly ordered samples at various temperatures down to 8 K. The observed, strongly texture-dependent properties are compared to both molecule based and band-structure calculations highlighting the influence of strongly anisotropic optical constants on the shape of the absorption spectra.

II. EXPERIMENTAL AND THEORETICAL METHODOLOGY

For our investigations we use para-sexiphenyl (6*P*) from Tokyo Chemical Industries Co. Ltd. The material is evaporated in high vacuum onto different substrates under various evaporation conditions as is listed in Table I. Highly ordered films of 6*P* with the molecular axes pointing in a single direction parallel to the substrate surface have been obtained by film growth on preoriented 6*P* nucleation centers (film *A*).[8,17] This is achieved by first evaporating a 6*P* layer with a thickness of about 5 nm. This film then is gently rubbed in one direction with wiping paper and subsequently another 110 nm of sexiphenyl are deposited. During the evaporation process the sample is kept at ambient temperature, because it has been shown that an increased substrate temperature favors the alignment of the 6*P* chains perpendicular to the film surface[11] resulting in a reduced anisotropy with respect to the rubbing direction. In our studies we have used various kinds of substrate materials (ITO, quartz, NaCl) but the highest degrees of anisotropy have been obtained using a NaCl crystal rubbing in the [100] crystal direction and selecting a deposition rate between 0.1 and 0.2 nm/min. In order to grow films of high optical quality with chains parallel to the surface of the substrate but lacking an alignment in a certain direction, high evaporation rates and a quartz substrate are chosen and the substrate is kept at room temperature during the evaporation process. Chains preferentially aligned perpendicular to the film surface are obtained at very low growth rates on heated substrates.[11,12] Free standing 6*P* films necessary for performing electron-diffraction experiments are achieved by floating films off NaCl substrates in distilled water and fixing them to electron microscopy grids.

Elastic electron-diffraction data are measured using the IFW Dresden transmission electron energy-loss spectrometer. A detailed description of the experimental setup is given elsewhere.[18] For x-ray diffraction a Siemens D 501 wide-angle x-ray diffractometer with Ni-filtered CuKα radiation is used. In this context it has to be noted that the electron-diffraction experiments are recorded in transmission whereas x-ray diffraction is performed in a reflection geometry. Therefore, the peaks that for a certain texturing are maximized in x-ray spectra vanish for electron diffraction and vice versa. The morphology of the films is determined using a Nanoscope III atomic force microscope (AFM) in tapping mode.

The absorption in the infrared range is investigated as a function of polarization by a Bomem MB 102 FTIR spectrometer equipped with a gold wire-grid polarizer. Anisotropic optical absorption spectra in the ultraviolet (UV/VIS) spectral range are recorded with a Perkin Elmer λ-9 two-

beam spectrometer equipped with a Hanle prism depolarizer (to compensate for the intrinsic polarization of the monochromator) and with a Glan Thompson prism polarizer. This polarizer limits the spectral range in the UV region to 300 nm (4 eV). For photoluminescence emission and excitation spectra a 1000-W Osram Xe lamp and a Jobin Yvon double monochromator H 10 D UV together with a Hanle prism depolarizer are used for the excitation. In order to record the polarized photoluminescence emission of a 6*P* film the light emitted from the backside of the sample is collected by an optical fiber and analyzed with a Jobin Yvon HR 640 high-resolution monochromator equipped with a Hamamatsu R943-02 photomultiplier detector. The photomultiplier is protected from primary radiation by an edge filter. To polarize the exciting radiation and to analyze the emitted light, foil polarizers are used. The spectra are corrected for the spectral intensity distribution of the lamp and the wavelength dependent absorption of the substrate and the foil polarizers.

Polarization dependent optical transitions for 6*P* molecules are calculated by an intermediate neglect of differential overlap (INDO)[19] approach coupled to a single configuration interaction (SCI) technique[20] to account for electron correlation effects. The geometry of the molecule is calculated by the Hartree-Fock semiempirical Austin Model 1 (AM1) technique, which provides good estimates of geometries and heats of formation for organic molecules in their ground state.[21] To account for packing effects in the solid state the inter-ring twist angles in the molecular calculations are set to 18° according to the DFT based geometry optimizations for the parent polymer poly(para-phenylene) in Ref. 22 (instead of the 40° obtained for fully AM1 geometry optimized isolated oligophenylenes[23]). For an inter-ring twist angle fixed at 22.7° as derived from x-ray diffraction experiments[24] similar results are obtained. In addition to the calculations for isolated molecules we have performed INDO/SCI based calculations for a variety of clusters containing up to six interacting 6*P* chains.

To be able to estimate the influence of correlation effects in the ground state and to allow a consistent comparison of the results obtained for molecules and molecular clusters with those from DFT-based band-structure calculations, we have also simulated the optical absorption of isolated and interacting 6*P* chains by molecule-based DFT methods. Due to the large size of the investigated systems the self-consistent field cycle is run with the Vosko-Wilk-Nusair[25] local potential. The nonlocal exchange and correlation energies are then calculated as a perturbation on the converged local-density approximation (LDA) density. Here the generalized gradient approximation for the correlation functional by Perdew and Wang[26] and the gradient corrected exchange functional by Becke[27] are used. Further methodological details are described in Ref. 28.

In order to gain a better understanding of the influence of three-dimensional (3D) interchain interaction effects, we have compared experimental data and molecule-based simulations to the results of band-structure calculations for crystalline 6*P*. They are performed by applying the linearized augmented plane wave (LAPW) method within density functional theory assuming a monoclinic space group with planar 6*P* chains in the unit cell.[29,30] For exchange and correlation effects LDA is used. An underestimation of the energy gap is a well-known effect in DFT results.[22] Calculations of the electron self-energies, however, have shown that for many materials the true quasiparticle bands differ from the LDA bands predominantly by a rigid upward shift of the conduction bands.[31] In addition to this, calculations for several polyenes have shown that a very good approximation for the relationship between the LDA energy gap and the experimental result is given by:[32]

$$E_{\mathrm{gap(LDA)}} = 0.6 E_{\mathrm{gap(experiment)}}. \tag{1}$$

Therefore the dielectric tensor calculated from the band structure is shifted by an appropriate energy (in the case of 6*P* by 1.4 eV). This modified dielectric tensor is subsequently used to determine the absorption coefficient of a 6*P* film as a function of the angle between the molecular axis and the wave vector of the transmitted light (see Refs. 14 and 33).

III. RESULTS AND DISCUSSION

A. Structure and texturing—elastic electron and x-ray diffraction

Depending on the evaporation conditions, 6*P* can adopt two crystallographic phases[12(a)] in the following denoted by β and γ. In the monoclinic β phase the angle between the molecular axis and the *ab* plane is 72° and the dimensions of the unit cell are $a = 8.091$ Å, $b = 5.568$ Å, $c = 26.241$ Å, and the monoclinic angle $\beta = 98.17°$ (Ref. 34, see also Ref. 35). A calculation of the positions of the diffraction peaks and intensities can be found in Ref. 36. In the γ phase the sexiphenyl chains are aligned perpendicular to the *ab* plane, mainly resulting in a shift of the $(00l)$ reflections to lower scattering angles.[37] The dimensions of the corresponding orthorhombic unit cell (containing twice the number of 6*P* molecules compared to the monoclinic cell) have been determined to be $a = 7.76$ Å, $b = 5.53$ Å, and $c = 54.6$ Å.[38] The Miller indices, interplanar spacings, positions of the peaks in reciprocal space, relative intensities calculated for x-ray diffraction at randomly distributed sexiphenyl crystallites, as well as the angles between the corresponding vectors in reciprocal space and the sexiphenyl chains for the β phase are listed in Table II for the most intense maxima. In Table III those peaks are listed whose intensities are strongly increased as a result of the texturing observed in sample *A* using electron diffraction. In this context, it has to be mentioned that only a qualitative comparison of the intensities calculated for x-ray diffraction with those measured by elastic electron diffraction can be performed because of different form factors and increased multiple-scattering probabilities for electron diffraction.

The elastic electron diffraction spectra for sample *A* are shown in Fig. 1 for various angles between the rubbing direction and the direction of momentum transfer. In the curve for 0° the intensities of the $(00l)$ peaks are strongly enhanced compared to the values calculated for an isotropic sample (Table II), whereas in the spectrum recorded with momentum transfer perpendicular to the preferred orientation, these peaks are not resolved. This and the fact that the (020) maximum is far more intense in the perpendicular geometry, indicate a good arrangement of the sexiphenyl

TABLE II. Most intense elastic-scattering peaks in an isotropic distribution of 6*P* crystallites. The intensities are calculated for x-ray diffraction in the β phase using single-crystal data (from Ref. 34). The details of the calculations are given in Ref. 36. The last column gives the angle between the normal to the crystallographic ab-plane and the orientation of the long axis of the 6*P* chains. Only planes with high corresponding diffraction intensities are listed.

Miller indices	Interplanar distance/Å	Peak position in reciprocal space/Å^{-1}	Relative intensity	Angle relative to 6*P* chains
(0 0 1)	25.97	0.24	321	18°
(0 0 2)	12.99	0.48	91	18°
(1 1 0)	4.57	1.37	97	76°
(1 1 $\underline{1}$)	4.57	1.38	1000	85°
(1 1 $\underline{2}$)	4.43	1.42	688	95°
(0 0 6)	4.33	1.45	102	18°
(2 0 $\underline{3}$)	3.85	1.63	765	90°
(2 1 $\underline{3}$)	3.17	1.99	606	90°

chains parallel to the preferred direction induced by the wiping process. To gain more insight into the orientation of the chains relative to the surface of the substrate we have measured the Bragg spectra for the sample being tilted around an axis parallel to the film surface but perpendicular to the rubbing direction. The strong dependence of a number of the peaks on this angle gives evidence of an alignment of the 6*P* chains parallel to the surface of the film with their axes aligned parallel to the direction of the rubbing process. For example the (203) and (016) peaks at 1.82 and 1.84 Å^{-1} have significantly increased intensities for the film being tilted by 40°. This is in full agreement with the above proposed texturing, as the angles between the vectors corresponding to those maxima in reciprocal space and the 6*P* chains are 40° and 42°, respectively. A similar observation is made for the (209), (20$\underline{1}$0), and (11$\underline{1}$1) reflections, which are most dominant in the spectrum measured for a tilt angle of about 20° in good agreement with the calculated angles between 15° and 22° (see Table III).

TABLE III. Elastic-scattering peaks in 6*P* that are enhanced due to texturing (film *A*). The relative intensities for x-ray diffraction of an isotropic distribution of crystallite orientations (see Ref. 36) are given for comparative reasons.

Miller indices	Interplanar spacing/Å	Position in reciprocal space/Å^{-1}	Relative intensities	Angle relative to 6*P* chains
(0 0 3)	8.66	0.73	41	18°
(0 0 4)	6.49	0.97	24	18°
(0 0 5)	5.19	1.21	23	18°
(2 0 3)	3.45	1.82	19	40°
(0 1 6)	3.42	1.84	16	42°
(2 1 3)	2.93	2.14	44	50°
(0 2 0)	2.78	2.26	9	90°
(0 2 6)	2.34	2.68	50	59°
(2 0 9)	2.20	2.86	11	15°
(2 0 $\underline{10}$)	2.05	3.06	23	13°
(1 1 $\underline{11}$)	2.03	3.10	20	22°

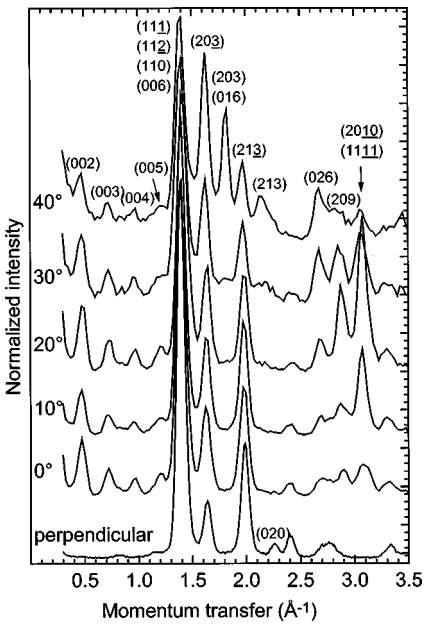

FIG. 1. Elastic electron-diffraction spectra of a highly-textured film of 6*P* grown on a preoriented 6*P* layer (film *A* from Table I) for various angles between the direction of momentum transfer and the preferred orientation induced by the rubbing process. The 0° scattering direction corresponds to momentum transfer in the rubbing direction and the curve denoted by ''perpendicular'' has been recorded with the scattering vector perpendicular to that direction but still in the plane of the substrate. To record the spectra for angles higher than 0°, the sample is tilted in a way that the vector of momentum transfer no longer lies in the plane of the film.

Elastic electron diffraction spectra for film *B* are shown in Fig. 2. The intensity of the (020) maximum strongly depends on the direction of momentum transfer (see inset of Fig. 2). The increased intensity of the (020) peak for certain directions compared to the calculated value in an isotropic sample (Table III) and the lack of intensity of the (00*l*) maxima are

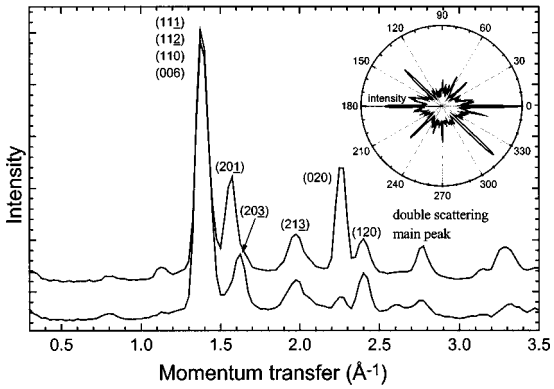

FIG. 2. Elastic electron-diffraction spectrum for a 6*P* film grown on a NaCl substrate at 150 °C with an evaporation rate of about 1 Å/min (film *B* in Table I). The upper spectrum is measured for a momentum transfer direction for which the (020) peak has a maximum (0°), whereas the lower spectrum is recorded at −5°, where the (020) peak becomes a minimum. For all spectra shown in this figure, the vector of momentum transfer lies in the plane of the substrate. In the inset the dependence of the (020) intensity on the direction of momentum transfer is shown.

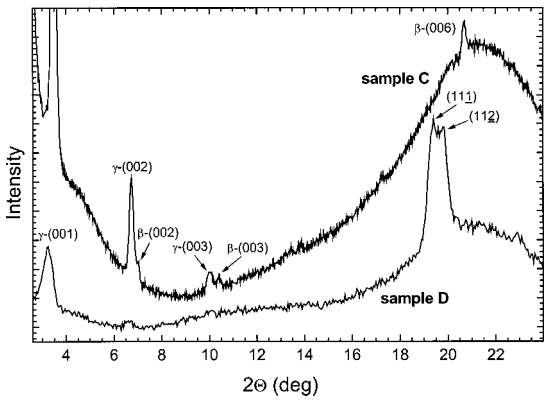

FIG. 3. X-ray diffraction spectra for 6*P* films deposited on quartz substrates at 100 °C with a deposition rate of 1 Å/min (sample *C*) and with the substrate held at ambient temperature and a deposition rate of about 200 Å/min (sample *D*). The broad maximum around 21° is due to scattering in the amorphous quartz substrate and the broad shoulder at low-diffraction angle results from forward scattering in air.

a strong indication for an alignment of the *ab* planes of the crystallites parallel to the surface of the film. This results in an angle of 72° between the film surface and the sexiphenyl chains in film *B* for crystallites of the β phase and a perpendicular alignment in the γ phase. Due to the reduced resolution of our electron diffraction experiments compared to x-ray diffraction (see below) it is not possible to distinguish between these two phases. Strong maxima of the (020) peak are observed at angles of 0°, (45°), 135°, 180°, 225°, and 315° (see inset of Fig. 2). This is an evidence for quasiepitaxial growth of 6*P* crystallites on the NaCl (100) planes with their *b* axis parallel to the ⟨100⟩ and ⟨110⟩ directions as reported also in Ref. 39. Yase *et al.*[40] have also observed an alignment of the *b* axis parallel to the ⟨110⟩ directions of various *bcc* crystal substrates. The fact that there are no maxima observed at 90° and 270° is a result of the reduced resolution and sensitivity of the spectrometer in those directions.

To determine UV/VIS properties of 6*P* we have also investigated thin films on quartz substrates (sample *C* and sample *D*). Their structure is determined by x-ray diffraction in reflection. The spectra obtained for sample *C* and sample *D* are shown in Fig. 3. At low-evaporation rates and high-substrate temperatures (sample *C*) only the (00*l*) reflections have significant intensities. This shows that in this film the *ab* planes of the crystallites are parallel to the substrate surface as in sample *B*.[12] The double structure of the peaks is a result of the polymorphism of sexiphenyl discussed above (appearance of β and γ phases). An exact quantification of the ratio of the two phases is not possible, as there are no single crystal data for the γ phase available in the literature. For film *D* a texturing with the (11-1) and (11-2) planes parallel to the substrate is dominant, which corresponds to sexiphenyl chains lying in a plane parallel to the film surface.[41] Additionally a portion of crystallites in the γ phase with the molecular axes perpendicular to the substrate is contained in the sample as is indicated by the strong γ (001) peak. These crystallites are presumably formed at the beginning of the deposition process, when the deposition rate has not yet reached its steady-state value.

Investigations of liquid-crystalline materials[42] have shown that the size of the region of coherent scattering in polymeric materials can be a measure of the obtained conjugation lengths essential to gain a deeper understanding of a material's photophysics. An x-ray line profile analysis performed for 6*P* in Ref. 43 does, however, show that internal disorder plays only a *minor role* in 6*P* molecular crystals. Therefore, it is reasonable to assume that the conjugation length in this material is determined by the size of the molecules. For films grown at ambient temperature and low-deposition rate (0.6 nm/min) (comparable to film *A* of our investigations) the crystallite size is the main contribution to line broadening in x-ray investigations. The typical crystallite size ranges from 40 to 150 nm. For films grown at elevated temperature—substrate at 170 °C—no contribution of the crystallite size to the width of the diffraction peaks has been observed, indicating regions of coherent scattering extending over several μm—compare Fig. 4(b).

B. Morphology of 6*P* films on NaCl substrates

The morphologies of films *A* and *B* have been investigated by tapping-mode AFM. The micrographs are shown in Figs. 4(a) and 4(b), respectively. As can be seen in Fig. 4(a), the nominally 120 nm thick film *A* (value determined using a microbalance) exhibits no obvious morphological anisotropy on the surface, although the molecular orientation is highly anisotropic with 6*P* chains lying parallel to the preferred direction induced by the rubbing process. One can observe distinct columnar grains with a typical diameter of 1200 Å and the mean surface roughness is estimated to be smaller than 200 Å. These observations are reminiscent of the morphological features observed for 6*P* films evaporated at higher rates on a variety of substrates not covered by an order inducing layer.[11,44] In these films, like in sample *A*, the 6*P* chains lie in a plane parallel to the surface of the substrate. Thus, columnar grains can be regarded as the characteristic morphology of 6*P* films with molecules lying parallel to the surface of the substrate regardless of any additional texturing.

A totally different behavior is found for film *B*, for which the substrate has been heated during the evaporation (see Table I). Figure 4(b) shows large, flat domains atop each other. A cross section reveals that the height of the terraces corresponds to the length of one 6*P* molecule, confirming the results of electron diffraction regarding the texturing of the film. The fact that we have been able to simultaneously observe terraces corresponding to six monolayers of 6*P* with a width of approximately 1 μm for each of the terraces, indicates the well-defined growth of 6*P* for low-evaporation rates and high-molecular mobilities resulting from an elevated temperature (150 °C) during the evaporation process. The large size of the crystallites in that film (bigger than the area shown in the micrograph) is in excellent agreement with results from line profile analysis of a 6*P* film evaporated at comparable conditions (see above).[43]

C. Absorption in the infrared range

The infrared absorption spectra of sample *A* for polarizations parallel and perpendicular to the rubbing direction and of sample *B* (measured without wire-grid polarizer) are con-

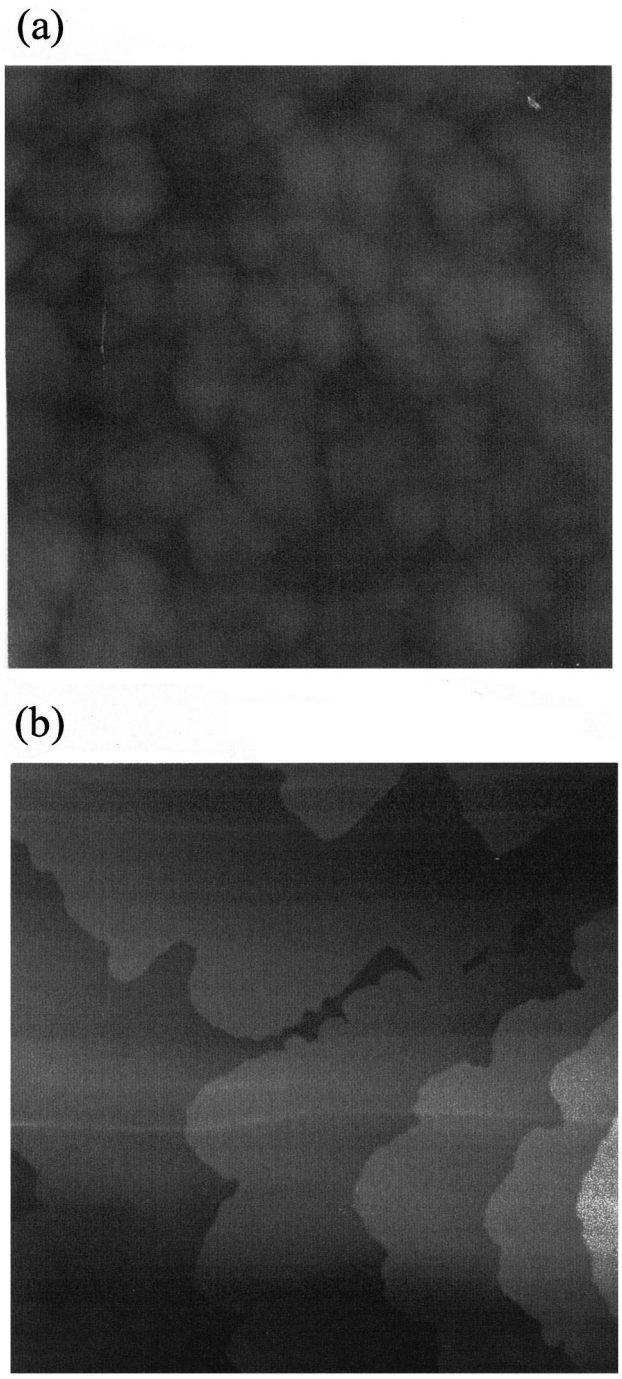

FIG. 4. (a) AFM micrograph of film *A*, one side of the image corresponds to 1.5 μm. The mean surface roughness is estimated to be smaller than 200 Å. (b) AFM micrograph of film *B*, one side of the image corresponds to 4.5 μm. The height of the terraces approximately corresponds to the length of the 6*P* molecules (28 Å).

tained in Fig. 5. The strongest maxima are situated at 759 cm^{-1} (attributed to the C-H out-of-plane bending vibration at the monosubstituted phenylene rings terminating the sexiphenyl molecule), at 813 cm^{-1} (related to C-H out-of-plane deformation of the para-substituted rings) and at 1480 cm^{-1}, the latter usually being attributed to C-C stretching vibrations.[45,46] Similar spectra have been obtained for films deposited from poly(para-phenylene) (PPP) powders.[47] Theoretical calculations of the normal modes and their intensi-

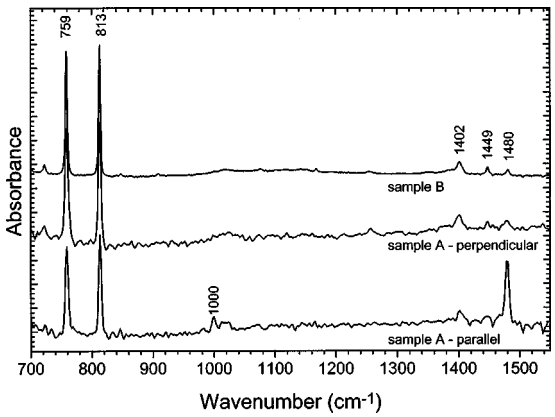

FIG. 5. Infrared-absorption spectrum for a highly ordered 6*P* film (sample *A*) parallel and perpendicular to the preferred orientation and for a film with the molecular axis oriented quasiperpendicular to the substrate surface (sample *B*—measured without wire-grid polarizer).

ties performed for a planar model of PPP (Ref. 48) however show that the 1480 cm^{-1} vibration involves also deformations of the C-C-H angles. The weaker peaks at 1000, 1402, and 1448 cm^{-1}, according to Refs. 45 and 46, are related to deformations similar to the 1480 cm^{-1} maximum.

As far as the polarizations of the transitions are concerned the calculations in Ref. 45 indicate that the 1480-cm^{-1} peak corresponds to electric dipole moment oscillations in the direction of the molecular axis and that the 813-cm^{-1} peak is polarized perpendicular. The fact that the maximum at 1480 cm^{-1} is very weak in film *B*, in which the chain axes are tilted by only 18° relative to the surface normal, as well as in film *A* for a polarization perpendicular to the preferred orientation of the molecular backbone, is in excellent agreement with the theoretical predictions. The maximum at 1000 cm^{-1}, is as well, polarized parallel to the molecular axis. The 813-cm^{-1} mode, however, is also strongly excited, when the incident radiation is polarized parallel to the molecular axes (film *A*). The reason for that is not fully understood yet. One possible explanation is that the vibration corresponding to the 813 cm^{-1} peak also contains significant contributions of in-plane motions possibly related to a deviation from the planar geometry assumed in the calculations in Ref. 45.

D. Quantum chemical simulations and DFT band-structure calculations

To gain a more profound understanding of the UV/VIS optical spectra and to assign the optically allowed transitions in 6*P* molecules to excitations between specific electronic states, we have performed quantum-chemical simulations of the absorption spectrum of 6*P* including electron correlation effects via a configuration interaction (CI) approach. This approach proved very successful in describing the electronic properties of neutral and doped oligophenylenes with varying chain lengths and yields an excellent agreement between the calculations and spectra measured in solution.[23] A comparison of molecule-based calculations and DFT band-structure derived optical absorption spectra with experimental data obtained for various 6*P* thin films, then allows to distinguish between features related to the intrinsic proper-

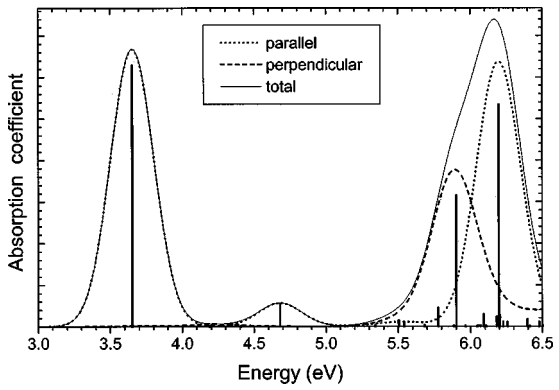

FIG. 6. INDO/SCI calculated absorption spectrum of a single $6P$ chain with the geometry optimized at the semiempirical AM1 level (the inter-ring twist angle being kept at 18°) for the electric-field vector polarized parallel and perpendicular to the molecular axis. In addition to the spectra obtained by a Gaussian broadening, also the discrete excited state energies with the corresponding oscillator strengths are shown as bars.

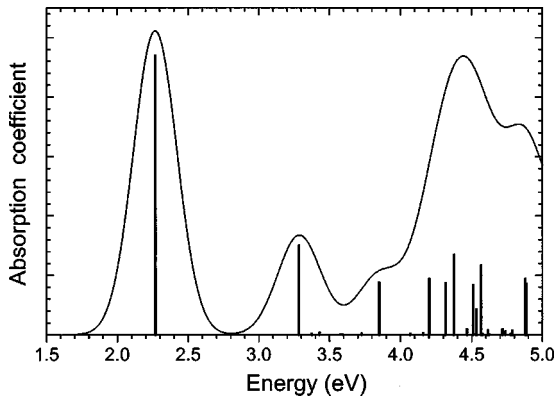

FIG. 7. Total optical absorption spectrum of an isolated $6P$ molecule calculated by density functional theory. The geometry is taken from Ref. 34 and subsequently refined by a geometry optimization in the crystalline environment. In addition to the spectra obtained by a Gaussian broadening, also the discrete excited state energies with the corresponding oscillator strengths are shown. The gap energy is strongly underestimated as it is usually observed for DFT calculations.

ties of $6P$ molecules and effects resulting from interchain interactions and the three-dimensional structure of $6P$ molecular crystals.

The INDO/SCI derived absorption spectrum of a $6P$ molecule with an inter-ring twist angle of 18° is shown in Fig. 6. When performing a quantitative comparison between the calculated peak positions and experimental spectra it has to be considered that interchain interactions result in a blueshift of the low-energy absorption feature as has been shown on the INDO/SCI level for phenylenevinylenes.[49] We have observed the same trend, when extending our calculations to clusters of $6P$ molecules.[50] An investigation of the excited states contributing to the absorption maxima (Table IV) shows that the lowest-energy transition is polarized parallel to the molecular axis and dominated by a single configuration, namely, a transition from the highest occupied molecular orbital (HOMO) to the lowest unoccupied molecular orbital (LUMO). This justifies a characterization of that excitation process in a single-particle description as it is e.g., done below when applying density functional theory.[51] The calculations predict a second rather weak parallel polarized transition at 4.68 eV, which involves similarly weighted contributions from excitations from the HOMO-2 to the LUMO, from the HOMO-1 to the LUMO$+1$, and from the HOMO to the LUMO$+2$. In the higher-energy range there is a maximum polarized perpendicular to the molecular axis, which corresponds to a highly-correlated excited state containing contributions of several transitions between localized and delocalized orbitals. Localized in this context means orbitals with vanishing electron density at the C atoms forming the inter-ring bridges, whereas delocalized refers to states with high-charge density at the bridging C atoms.[52] The parallel polarized peak at 6.2 eV can be attributed to transitions between localized levels.[53]

Molecule-based calculations carried out in the framework of density functional theory yield equivalent results, as is shown in Fig. 7 for an isolated $6P$ chain. They allow a more direct comparison to the DFT-based band-structure calculations discussed below, because both methods rely on the same theoretical framework. The molecular geometry here is taken from Ref. 34 and in a second step refined by DFT-based geometry optimizations in the crystalline environment for a planar molecule—i.e., it is the same molecular geom-

TABLE IV. INDO/SCI transition energies, polarization relative to the molecular axis, oscillator strengths and main CI expansion coefficients for the low-lying absorption peaks in $6P$ with an interring twist angle set to 18°. (H corresponds to the HOMO and L to the LUMO.)

Energy (eV)	Oscillator strength (arb. units)	Polarization	Main CI expansion coefficients
3.65	2.87	$\parallel$	$0.89[H\rightarrow L]-0.37[H-1\rightarrow L+1]$
4.68	0.24	$\parallel$	$0.64[H\rightarrow L+2]+0.54[H-1\rightarrow L+1]$ $+0.41[H-2\rightarrow L]$
5.90	1.44	$\perp$	$0.49[H\rightarrow L+8]-0.39[H-8\rightarrow L]$ $-0.35[H\rightarrow L+6]+0.29[H-7\rightarrow L+1]$
6.20	2.44	$\parallel$	$-0.41[H-8\rightarrow L+8]-0.35[H-6\rightarrow L+6]$ $-0.35[H-7\rightarrow L+7]$ $-0.35[H-3\rightarrow L+3]+0.35[H-5\rightarrow L+5]$ $+0.31[H-4\rightarrow L+4]$

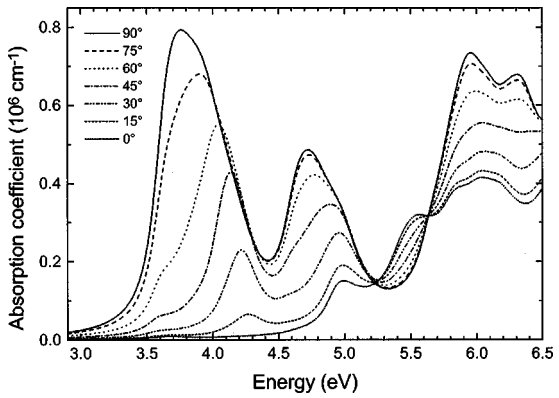

FIG. 8. Dependence of the optical-absorption spectrum of 6*P* on the angle between the wave vector of the transmitted light and the long molecular axis as derived from corresponding band-structure data. (Note: An angle of 90° between the molecular axis and the wave vector of the incident light corresponds to an optical transition moment parallel to the 6*P* chains.) To ease the comparison with experimental data, a Gaussian broadening with a full width at half maximum of 0.2 eV has been applied to the calculated dielectric functions. For the depicted absorption coefficients the plane of polarization corresponds to the plane formed by the incident light and the chain axis.

etry, which in the following is used for the band-structure calculations (see Ref. 29). The calculated transition energies are too low, as it has to be expected for DFT calculations (see methodology section). According to Eq. (1) the DFT derived HOMO-LUMO separation has to be increased by 1.5 eV, which then yields an absorption spectrum reminiscent of that obtained in the INDO/SCI calculations in Fig. 6. Like in the INDO/SCI calculations the lowest-excited state is characterized by the HOMO→LUMO transition. In the higher-energy range there is a large variety of excited states with significant oscillator strengths. In the INDO/SCI description these excitations are coupled by configuration interaction giving rise to the two states at 5.9 and 6.2 eV, respectively. The very good agreement between the highly correlated INDO/SCI calculations and the molecule-based DFT simulations, especially in the low-energy region, are another indication that band-structure calculations performed in a single-particle picture are a useful tool to both qualitatively and also quantitatively understand the optical properties of the 6*P* molecular crystals.

In order to properly describe absorption processes in an anisotropic medium and to fully consider the actual three-dimensional structure of 6*P* molecular crystals, DFT band-structure calculations, considering the periodicity of the investigated materials in all three dimensions of space, have been performed.[29] In this paper we present calculations of the optical properties of 6*P*, which have been derived from corresponding band-structure data. Following the relationship between optical absorption and the dielectric tensor of an anisotropic medium[54] (see e.g., Ref. 55 and the review given in Ref. 33) the optical absorption spectrum of 6*P* has been calculated as a function of the angle Θ between the molecular axis and the wave vector of the transmitted light.[56] The results are shown in Fig. 8.

The principal features obtained from the band-structure calculations are equivalent to those derived from the molecule-based simulations shown in Figs. 6 and 7: There is a pronounced peak between 3.5 and 4.0 eV and another maximum around 4.7 eV, for which the highest oscillator strengths are obtained, when the electric field is polarized parallel to the molecular axis ($\Theta = 90°$); the maximum around 5.5 eV is polarized perpendicular to the molecular axis and at higher energies there are several intense peaks polarized parallel. The consideration of the full three-dimensional anisotropic nature of the 6*P* molecular crystal gives, however, rise to an effect that is not expected when relying on simple (e.g., molecule based) models: For the lowest-lying maximum a decrease of the angle between the direction of light propagation and the molecular axes Θ (which is accompanied by an increase of the angle between the electric field and the chain direction) does not only result in a reduction of the oscillator strength of the transition, but also leads to a shift of the position of the peak. In this context it is important to point out that the observed shift is a consequence of the complex wave propagation properties induced by the marked anisotropy of the absorbing 6*P* molecular crystal.[33] It is NOT related to a perpendicularly polarized maximum at slightly higher energies than the main peak (which could gain intensity upon decreasing Θ), as there is no such transition in 6*P*. This can be concluded from the fact that for $\Theta = 0°$ there is virtually no absorption below 4.5 eV.

E. Optical properties

The optical absorption spectra of the highly ordered film *A* in the UV/VIS range are shown in Fig. 9 for room temperature (top) and at 8 K (bottom). They indicate a strong anisotropy of the transition matrix elements associated with the lowest-energy transition (well resolved as a peak at 3.35 eV in the low-temperature experiments) as a function of the angle between the plane of polarization and the molecular axis. This peak in the molecular picture can be attributed to one of the vibronic bands of the first excitation dominated by a transition from the HOMO to the LUMO. The INDO/SCI simulations as well as the DFT-based molecular- and band-structure calculations show that the lowest-energy transition is polarized parallel to the molecular axes in agreement with the experimental observations. In this context it is important to point out that for the texturing determined for film *A*, only the angle between the vector of the electric field and the molecular axis changes, when varying the plane of polarization. The angle between the molecular axis and the wave vector of the incident light remains the same. This explains, why no shift of the peaks is observed in Fig. 9. The gradual onset of the spectra shown in Fig. 9 and the monotonous increase of the absorption coefficient at higher energies, are related to scattering of light in the slightly opaque film grown on the NaCl crystal (film *A*).

The photoluminescence excitation and emission spectra[57] for film *A* (measured at ambient temperature) are shown in Fig. 10 for excitation and emission polarizers, both parallel (solid line) and both perpendicular (dashed line) to the preferred orientation of the 6*P* chains. The spectra show the very high anisotropy achieved in this film. So for example, the photoluminescence emission intensity at 2.92 eV in the parallel/parallel alignment is a factor of 9.2 higher than for

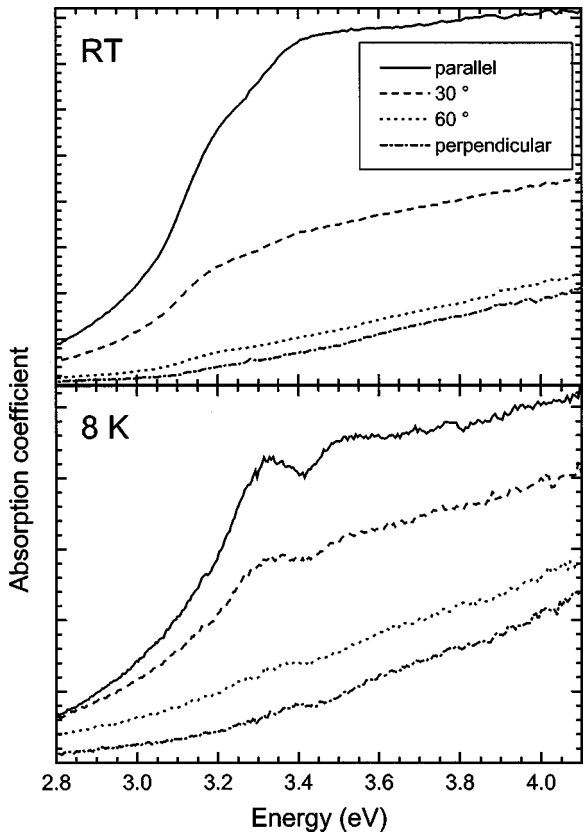

FIG. 9. Optical absorption of a highly-oriented film of 6*P* on NaCl (sample *A*) as a function of the angle between the polarization of light and the chain direction measured at room temperature (top) and at 8 K (bottom).

both polarizers perpendicular to the chain axes. The highest anisotropy in the excitation spectrum is achieved at 3.41 eV. At that energy the parallel/parallel excitation efficiency is a factor of 6.6 higher than the perpendicular/perpendicular one. The only minor influence of scattering effects on excitation spectra explains the relatively sharp onset of the excitation profiles in Fig. 10 compared to the absorption spectra

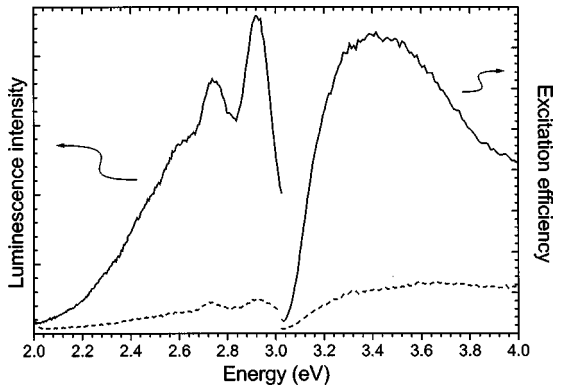

FIG. 10. Excitation and emission spectra of a highly ordered 6*P* film (sample *A*) for excitation and emission polarizers both parallel (solid line) and both perpendicular (dashed line) to the rubbing direction. For the excitation spectra the emission energy is set to 2.76 eV (450 nm) and for the emission spectra the sample is excited at 3.44 eV (360 nm). The spectra are recorded at ambient temperature.

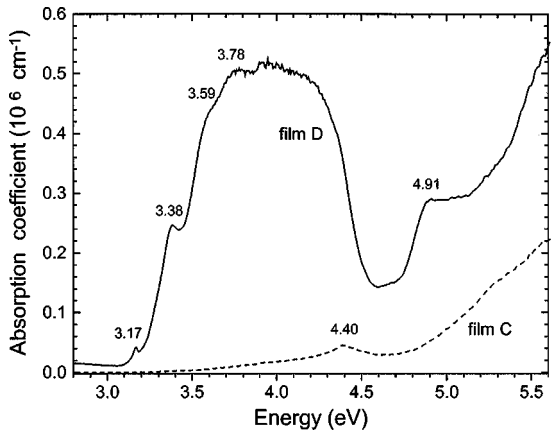

FIG. 11. Optical absorption of 6*P* films on quartz at 7 K (measured without polarizer to extend measuring range—see methodology section). In film *D* the 6*P* molecular axes predominantly lie in the plane of the substrate, whereas in film *C* they are oriented mainly perpendicular to it. [The small step at 3.9 eV is an artifact of the experimental set up and the low signal-to-noise ratio between 3.8 and 4.1 eV is a result of the low transmission of the sample in that energy range ($T \approx 0.5\%$).] The thickness of the films necessary to determine the absolute values of the optical absorption has been determined by a Tolansky interferometer.

in Fig. 9 and can also be regarded to be one of the reasons for the deviations between the absorption and excitation spectra in the higher-energy range.

To grow films with higher optical quality in order to better resolve the actual shape of the spectra, quartz substrates have been used. The absorption coefficients obtained for film *C* and film *D* at a temperature of 7 K are shown in Fig. 11 (spectra measured without polarizer to extend the measuring range—see methodology section). As the spectrum of film *D* is dominated by crystallites in which the sexiphenyl chains lie in a plane parallel to the film surface (see Sec. III A) a strong contribution of transitions with transition dipole moments parallel or nearly parallel to the molecular axis is observed. Peaks and shoulders at 3.17, 3.38, 3.59, and 3.78 eV are well resolved. The maxima at 3.38, 3.59, and 3.78 eV can be regarded as vibronic replicas of the lowest-energy transition at 3.17 eV, with the 3.38 eV maximum corresponding to the peak observed in sample *A*. An attribution of these features to a vibronic progression is supported by the similar energetic distances between the maxima. Theoretical calculations predict an intense Raman active mode for planar (PPP) between 0.200 and 0.206 eV,[58] which is related predominantly to C-C stretching vibrations involving all carbon atoms of the molecule. Experimental Raman spectra yield a slightly lower energy of 0.197 eV both for 6*P* and PPP.[46,59] The strong coupling of this mode to the electronic transition, which is emphasized by the relatively low intensity of the 0-0 transition with respect to the higher-lying replicas, indicates a significant modification of the molecular backbone as a result of the excitation process. This is due to the more quinoidal character of the singlet excited state.[60] The slightly higher energy observed in the vibronic progression of the absorption spectrum compared to the Raman data can be explained by the fact that for an absorption process the coupling to vibrations of the singlet excited state is crucial, whereas Raman experiments probe the vibrational properties of the ground state.

The broad absorption spectrum in $6P$ and $6T$ films compared to planarized and isolated moieties[5(a),6,61,62] can be explained by several effects: (i) In not chemically bridged materials and systems that are not planarized by strains imposed by a matrix material, in addition to the stretching vibrations, there is also a strong coupling to torsional vibrations. They usually cannot be resolved experimentally due to the low energy of the associated phonons. These torsional vibrations then result in a smearing out of the vibronic structure originating from the stretching vibrations. (ii) The electronic bands in molecular crystals involved in the absorption process have a finite width due to the three-dimensional geometric structure, whereas in isolated molecules one is dealing with electronic transitions between discrete molecular levels. (iii) The actual absorption spectrum of a molecular crystal strongly depends on the orientation of the crystallites and is influenced by the complex dielectric properties of the optically anisotropic systems as shown in Fig. 8. (iv) Due to the presence of two inequivalent chains in the $6P$ as well as in the $6T$ unit cells, both the conduction and valence bands are split. Therefore, the absorption spectrum is a superposition of the transitions between these bands. The band-structure calculations in Ref. 29 also indicate that the gap between electronic states with a wave-number vector perpendicular to the molecular axis at the borders of the first Brillouin zone is comparable to that at the Γ point (wave vector$=0$). These ''broadening effects'' and the resulting complex nature of the broad absorption feature imply that one cannot directly compare the intensities of the different vibronic peaks to determine, for example, the Huang-Rhys parameter related to the C-C stretching vibrations.

The absorption spectrum of film *C* in Fig. 11 completely lacks the transition at 3.17 eV and its vibronic progression. Instead there is a peak at 4.40 eV, for which there is no equivalence in the molecular simulations in Figs. 6 and 7. (In the molecular picture all transitions below 5.9 eV are polarized in the direction of the $6P$ chains.) However, the calculations in Fig. 8 predict an absorption in that energy range for low angles between the direction of the wave vector and the molecular axis. This is a consequence of the shift of the low-energy peak upon decreasing Θ in Fig. 8. The observations are consistent with the results of the x-ray diffraction studies described above, which for film *D* predict for part of the crystallites a tilt angle of 18° between the $6P$ molecular axes and the surface normal (β phase).[63] According to Fig. 8 the $6P$ chains crystallized in the γ phase do not contribute to the low-energy part of the absorption spectrum. The lack of any vibronic structure of the 4.40 eV peak is in marked contrast to the properties of the lower-lying excitations in film *C*.

The fact that depending on the orientation of conjugated organic molecules in thin films, strong differences of the absorption spectrum are observed, has also been explained by exciton interactions between neighboring molecules in the crystalline environment.[15] The coupling between the transition dipole moments of molecules at crystallographically inequivalent sites resulting from the herringbone alignment of the chains in the unit cell leads to Davydov splitting. Recent combined experimental and theoretical[64] investigations for sexithienyl ($6T$) have, however, shown that the Davydov splitting accounts for a very weak transition polarized perpendicular to the molecular axis, which is only 0.3 eV, *below* the dominant low-energy excitation.[65] The Davydov splitting, therefore, cannot account for the 4.40-eV peak seen in the absorption spectra of $6P$ films with molecular axes quasiperpendicular to the substrate surface (Fig. 11).

IV. CONCLUSIONS

By varying the deposition conditions of $6P$ on a number of substrates we have obtained highly textured thin films allowing an investigation of the polarization dependent properties of that material. Evaporating $6P$ at low rates onto heated substrates yields films with the molecular axes nearly perpendicular to the film surface. For such samples AFM investigations show a layered film growth. For substrates kept at room temperature the $6P$ molecules lie parallel to the substrate and a deposition on a preoriented $6P$ layer yields a high degree of anisotropy as shown by elastic electron diffraction and polarization dependent IR absorption as well as photoluminescence excitation and emission measurements in the visible range.

The shape of the absorption spectra strongly depends on the actual texturing of the film. Polarization dependent absorption measurements clearly show that the lowest-energy transition is polarized parallel to the molecular axis, in full agreement with molecule-based calculations. Electron-energy-loss spectroscopy (EELS) experiments and simulations of the inelastic-scattering spectra indicate that the basic electronic structure of molecular crystals can be derived from the properties of the individual building blocks.[39,66] A detailed analysis of the absorption spectra, however, shows that their shape is significantly influenced by bulk effects. The comparison between the experimental data and theoretical calculations based on DFT band-structure results shows that the different absorption spectra for sexiphenyl films evaporated under various conditions are a consequence of the alignment of the sexiphenyl chains relative to the direction of the incident light.

ACKNOWLEDGMENTS

We acknowledge the financial support by a Doktorandenstipendium of the Austrian Academy of Science, by the Spezialforschungsbereich Elektroaktive Stoffe of the Austrian Fonds zur Förderung der wissenschaftlichen Forschung and by a Förderungsstipendium of the Technische Universität Graz. We are also indebted to G. Jakopic for fruitful discussions and to G. Meinhardt, K. Reichmann, and W. Lukas for their support.

*Electronic address: Egbert@FFPHAL01.tu-graz.ac.at

[1] C. W. Tang and S. A. VanSlyke, Appl. Phys. Lett. **51**, 913 (1987); J. H. Burroughes, D. D. C. Bradley, A. R. Brown, R. N. Marks, K. Mackay, R. H. Friend, P. L. Burn, A. Kraft, and A. B. Holmes, Nature (London) **347**, 539 (1990); D. Braun and A. J. Heeger, Appl. Phys. Lett. **58**, 1982 (1991); R. H. Friend, R. W. Gymer, A. B. Holmes, J. H. Burroughes, R. N. Marks, C. Taliani, D. D. C. Bradley, D. A. dos Santos, J. L. Brédas, M. Lögdlund, and W. R. Salaneck, Nature (London) **397**, 121 (1999).

[2] Q. Pei, G. Yu, Ch. Zhang, Y. Yang, and A. J. Heeger, Science **269**, 1086 (1995); Q. Pei, Y. Yang, G. Yu, Ch. Zhang, and A. J. Heeger, J. Am. Chem. Soc. **118**, 3922 (1996).

[3] N. S. Sariciftci, L. Smilowitz, A. J. Heeger, and F. Wudl, Science **258**, 1474 (1992); J. J. M. Halls, C. A. Walsh, N. C. Greenham, E. A. Marseglia, R. H. Friend, S. C. Moratti, and A. B. Holmes, Nature (London) **376**, 498 (1995).

[4] F. Garnier, G. Horowitz, X. Peng, and D. Fichou, Adv. Mater. **2**, 592 (1990); F. Garnier, R. Hajlaoui, A. Yassar, and P. Srivastava, Science **265**, 1684 (1994); A. Dodabalapur, L. Torsi, and H. E. Katz, *ibid.* **268**, 270 (1995).

[5] (a) J. Stampfl, S. Tasch, G. Leising, and U. Scherf, Synth. Met. **71**, 2125 (1995); (b) Y. Yang, Q. Pei, and A. J. Heeger, J. Appl. Phys. **79**, 934 (1996).

[6] S. Tasch, A. Niko, G. Leising, and U. Scherf, Appl. Phys. Lett. **68**, 1090 (1996).

[7] Y. Ohmori, M. Uchida, K. Muro, and K. Yoshino, Jpn. J. Appl. Phys., Part 2 **30**, L1941 (1991); G. Grem, G. Leditzky, B. Ullrich, and G. Leising, Adv. Mater. **4**, 36 (1992); W. Graupner, G. Grem, F. Meghdadi, C. Paar, G. Leising, U. Scherf, K. Müllen, W. Fischer, and F. Stelzer, Mol. Cryst. Liq. Cryst. Sci. Technol., Sect. A **256**, 549 (1994); Y. Yang, Q. Pei, and A. J. Heeger, J. Appl. Phys. **79**, 934 (1996).

[8] M. Era, T. Tsutsui, and S. Saito, Appl. Phys. Lett. **67**, 2436 (1996).

[9] C. Kallinger, M. Hilmer, A. Haugeneder, M. Perner, W. Spirkl, U. Lemmer, J. Feldmann, U. Scherf, K. Müllen, A. Gombert, and V. Wittmer, Adv. Mater. **10**, 920 (1998); S. Stagira, M. Zavelani-Rossi, M. Nisoli, S. DeSilvestri, G. Lanzani, C. Zenz, P. Mataloni, and G. Leising, Appl. Phys. Lett. **73**, 2860 (1998).

[10] S. Tasch, C. Brandstätter, F. Meghdadi, G. Leising, G. Froyer, and L. Athouel, Adv. Mater. **9**, 33 (1997).

[11] R. Resel, N. Koch, F. Meghdadi, G. Leising, W. Unzog, and K. Reichmann, Thin Solid Films **305**, 232 (1997).

[12] L. Athouel, G. Froyer, and M. T. Riou, Synth. Met. **57**, 4734 (1993).

[13] H. Yanagi, S. Okamoto, and T. Mikami, Synth. Met. **91**, 91 (1997).

[14] A. Niko, F. Meghdadi, C. Ambrosch-Draxl, P. Vogl, and G. Leising, Synth. Met. **76**, 177 (1996).

[15] D. Fichou, G. Horowitz, B. Xu, and F. Garnier, Synth. Met. **48**, 167 (1992); F. Deloffre, F. Garnier, P. Srivastava, A. Yassar, and J.-L. Fave, *ibid.* **67**, 223 (1994); A. Yassar, G. Horowitz, P. Valat, V. Wintgens, M. Hmyene, F. Deloffre, P. Srivastava, P. Lang, and F. Garnier, J. Phys. Chem. **99**, 9155 (1995); M. Muccini, E. Lunedei, A. Bree, G. Horowitz, F. Garnier, and C. Taliani, J. Chem. Phys. **108**, 7327 (1998).

[16] D. Fichou, P. Demanze, G. Horowitz, R. Hajlaoui, M. Constant, and F. Garnier, Synth. Met. **85**, 1309 (1997).

[17] K. Erlacher, R. Resel, J. Keckes, and G. Leising, J. Cryst. Growth (to be published).

[18] J. Fink, Z. Phys. B: Condens. Matter **61**, 463 (1985); J. Fink, Adv. Electron. Electron Phys. **75**, 121 (1989).

[19] J. A. Pople, D. L. Beveridge, and P. A. Dobosh, J. Chem. Phys. **47**, 2026 (1967).

[20] A. Szabo and W. S. Ostlund, *Modern Quantum Chemistry: Introduction to Advanced Electronic Structure Theory* (Macmillan, New York, 1982).

[21] M. J. S. Dewar, E. G. Zoebisch, E. F. Healy, and J. J. P. Stewart, J. Am. Chem. Soc. **107**, 3902 (1985).

[22] C. Ambrosch-Draxl, J. A. Majewski, P. Vogl, and G. Leising, Phys. Rev. B **51**, 9668 (1995); C. Ambrosch-Draxl, J. A. Majewski, P. Vogl, G. Leising, R. Abt, and K. D. Aichholzer, Synth. Met. **69**, 411 (1994).

[23] E. Zojer, J. Cornil, G. Leising, and J. L. Brédas, Phys. Rev. B **59**, 7957 (1999).

[24] J. L. Baudour, H. Cailleau, and W. B. Yelon, Acta Crystallogr., Sect. B: Struct. Crystallogr. Cryst. Chem. **33**, 1773 (1977); J. L. Baudour, Y. Delugeard, and P. Rivet, *ibid.* **34**, 625 (1978).

[25] S. J. Vosko, L. Wilk, and M. Nusair, Can. J. Phys. **58**, 1200 (1980).

[26] J. P. Perdew and Y. Wang, Phys. Rev. B **45**, 13 244 (1992).

[27] A. D. Becke, J. Chem. Phys. **88**, 2547 (1998).

[28] E. Zojer, Ph.D. thesis, Technische Universität Graz, 1999.

[29] P. Puschnig and C. Ambosch-Draxl, Phys. Rev. B **60**, 7891 (1999).

[30] P. Blaha, K. Schwarz, and J. Luitz, *Wien 97, A Full Potential Augmented Plane Wave Package for Calculating Crystal Properties* (Karlheinz Schwarz, Techn. Universität Wien, Austria, 1999).

[31] X. Zhu and S. G. Louie, Phys. Rev. B **43**, 14 142 (1991).

[32] G. Brocks, P. J. Kelly, and R. Car, Synth. Met. **55-57**, 4243 (1993).

[33] P. Puschnig, Diploma Thesis, presented to the Technische Universität Graz, 1999.

[34] K. N. Baker, A. V. Fratini, T. Resch, H. C. Knachel, W. W. Adams, E. P. Socci, and B. L. Farmer, Polymer **34**, 1571 (1993).

[35] C. J. Toussaint, Acta Crystallogr. **21**, 1002 (1966).

[36] K. D. Aichholzer, Ph.D. thesis, Technische Universität Graz, 1995.

[37] R. Resel (unpublished).

[38] A. Kawaguchi, M. Tsuji, S. Moriguchi, A. Uemura, S. Isoda, M. Ohara, J. Petermann, and K. Katayama, Bull. Inst. Chem. Res., Kyoto Univ. **64**, 54 (1986).

[39] E. Zojer, M. Knupfer, R. Resel, F. Meghdadi, G. Leising, and J. Fink, Phys. Rev. B **56**, 10 138 (1997).

[40] K. Yase, E.-M. Han, K. Yamamoto, Y. Yoshida, N. Takada, and N. Tanigaki, Jpn. J. Appl. Phys., Part 1 **36**, 2843 (1997).

[41] R. Resel and G. Leising, Surf. Sci. **409**, 302 (1998).

[42] M. Grell, D. D. C. Bradley, G. Ungar, Hill, and K. S. Whitehead, Macromolecules **32**, 5810 (1999).

[43] H.-J. Brandt, R. Resel, J. Keckes, B. Koppelhuber-Bitschnau, N. Koch, and G. Leising, Mater. Res. Soc. Symp. Proc. **561**, 161 (1999).

[44] N. Koch, R. Resel, F. Meghdadi, G. Leising, and K. Reichmann, Synth. Met. **84**, 649 (1997).

[45] P. Kovacic and L.-C. Hsu, J. Polym. Sci., Part A 1 **4**, 5 (1996).

[46] G. Louarn, L. Athouel, G. Froyer, J. P. Buisson, and S. Lefrant, Synth. Met. **55-57**, 4762 (1993).

[47] K. Miyashita and M. Kaneko, Synth. Met. **68**, 161 (1995).

[48] D. Raković, I. Božović, S. A. Stepanyan, and L. A. Gribov, Solid State Commun. **43**, 127 (1982).

[49] J. Cornil, A. J. Heeger, and J. L. Bredas, Chem. Phys. Lett. **272**, 463 (1997); J. Cornil, D. A. dos Santos, X. Crispin, R. Silbey, and J. L. Brédas, J. Am. Chem. Soc. **120**, 1289 (1998).

[50] Calculations performed for 6*P* clusters with geometries derived from the crystal structure given in Ref. 34 (both for the INDO/SCI and the DFT approach) yield absorption spectra very similar to those shown in Figs. 6 and 7. There is no change in the shape of the spectra. The only difference is a small shift of the spectral features, which, e.g., in the INDO/SCI calculations is about 0.2 eV for the largest investigated cluster containing six interacting

6*P* chains. Clusters consisting of fully parallel 6*P* chains with AM1 optimized geometries yield equivalent results. The details of the cluster-based simulations are discussed in Ref. 28.

[51] In the DFT calculations for 6*P* presented in this paper correlation effects are not explicitly considered for the excited state via a CI but are only implicitly contained in the exchange correlation potential primarily designed to describe the ground state.

[52] P. Brocorens, E. Zojer, J. Cornil, Z. Shuai, G. Leising, K. Müllen, and J. L. Brédas, Synth. Met. (to be published).

[53] For the polarization of the peaks see also M. J. Rice and Yu. N. Gartstein, Phys. Rev. Lett. **73**, 2504 (1994).

[54] The reflection at the interfaces is not explicitly considered but hardly influences the shape of the absorption spectra.

[55] M. Born and E. Wolf, *Principles of Optics*, 3rd ed. (Pergamon, New York, 1965).

[56] As pointed out already above, the lowest-lying excited state in the highly correlated INDO/SCI molecular simulations is dominated by a single configuration. This implies that band-structure calculations relying on a single-particle picture should provide a proper description of the electronic structure of the organic molecular crystals. In a recent theoretical report [M. Rohlfing and S. G. Louie, Phys. Rev. Lett. **82**, 1959 (1999)] the authors do point to the significance of excitonic effects by solving the Bethe-Salpeter equation for *isolated* poly(acetylene) and poly(phenylene-vinylene) (PPV) chains. This approach can not be applied to the 6*P* molecular crystals investigated here, as first of all such calculations are far beyond present computational possibilities for the 6*P* unit cell containing 124 atoms. The inclusion of *interchain interaction* effects (in a crystalline environment) does, strongly reduce the exciton binding energy, as has been shown in J.-W. van der Horst, P. A. Bobbert, and M. A. J. Michels, Phys. Rev. Lett. **83**, 4413 (1999). Secondly the polarizations of some of the transitions for PPV in the paper by Rohlfing *et al.* do not agree with previous theoretical and experimental observations for phenylene containing materials. The polarizations of the transitions are, however, crucial for the effects discussed in this work.

[57] The degree of polarization of luminescence can be influenced either by exciton migration to domains with reduced orientation or by disorder within the individual crystallites. The latter effect does not play a significant role in 6*P* molecular systems, as has been discussed in the structure and texturing section. For 6*P* films grown at ambient temperature and low-deposition rates the typical crystallite size ranges from 40–150 nm,[43] which is of the same order of magnitude as the typical exciton diffusion length in organic molecular crystals [compare, e.g., M. Pope and C. E. Swenberg, *Electronic Processes in Organic Crystals* (Clarendon, New York, 1982) and references therein]. Therefore, a certain depolarization due to exciton migration between crystallites with different degrees of texturing cannot be excluded in those types of 6*P* films.

[58] G. Zannoni and G. Zerbi, J. Chem. Phys. **82**, 31 (1985); I. Božović and D. Raković, Phys. Rev. B **32**, 4325 (1985); L. Cuff and M. Kertesz, Macromolecules **27**, 762 (1994).

[59] Y. Furukawa, H. Ohta, A. Sakamoto, and M. Tasumi, Spectrochim. Acta A **47**, 1367 (1991); Y. Pelous, G. Froyer, C. Herold, and S. Lefrant, Synth. Met. **29**, E17 (1989).

[60] We have performed geometry optimizations for planar 6*P* based on the Austin Model 1 coupled to a CI description for the excited state. These calculations yield a reduction of 0.04 Å in the length of the central inter-ring bond in 6*P* in the lowest-lying excited state compared to the ground state.

[61] J. Stampfl, W. Graupner, G. Leising, and U. Scherf, J. Lumin. **63**, 117 (1995); G. Grem, C. Paar, J. Stampfl, and G. Leising, Chem. Mater. **7**, 2 (1995).

[62] G. Bongiovanni, C. Botta, G. Di Silvestro, A. Mura, and R. Tubino, Phys. Lett. A **208**, 165 (1995).

[63] In this context it is important to keep in mind that for perpendicular incidence the direction of the wave vector also inside an optically anisotropic medium is always perpendicular to the surface, independent of the orientation of the optical axes. (This does not apply, e.g., to the Pointing vector.) Therefore, one can directly compare the calculations from Fig. 8 to the experiments in Fig. 11.

[64] M. Muccini, E. Lunedei, C. Taliani, D. Beljonne, J. Cornil, and J. L. Brédas, J. Chem. Phys. **109**, 10 513 (1998).

[65] For recent experimental investigations on ultrathin oligothiophene films compare also W. Gebauer, M. Bässler, R. Fink, M. Sokolowski, and E. Umbach, Chem. Phys. Lett. **266**, 177 (1997); W. Gebauer, M. Sokolowski, and E. Umbach, Chem. Phys. **227**, 33 (1998).

[66] E. Zojer, Z. Shuai, G. Leising, and J. L. Brédas, J. Chem. Phys. **111**, 1668 (1999).